Composite Structures
DOI: 10.1016/j.compstruct.2020.113300

Microscale material variability and its effect on longitudinal tensile failure of unidirectional carbon fibre composites

Fabio Malgioglio[a,b,*], Soraia Pimenta[c], Anna Matveeva[a], Laszlo Farkas[a], Wim Desmet[d,e], Stepan V. Lomov[b], Yentl Swolfs[b]

[a]*Siemens Industry Software NV, Interleuvenlaan 68, 3001, Leuven, Belgium*
[b]*KU Leuven, Department of Materials Engineering, Kasteelpark Arenberg 44, 3001, Leuven, Belgium*
[c]*meComposites, Imperial College London, Department of Mechanical Engineering, South Kensington Campus, SW7 2AZ, London, UK*
[d]*KU Leuven, Department of Mechanical Engineering, Celestijnenlaan 300, 3001, Leuven, Belgium*
[e]*Flanders Make, DMMS Core Lab, Belgium*

Abstract

This paper deals with modelling the effect of local fibre volume fraction variability, fibre misalignment and fibre strength variability on the longitudinal tensile strength of unidirectional plies with finite element analysis. Variability is accounted for by generating spatially-correlated fields of fibre misalignment and volume fraction. This information is then translated into local mechanical properties and orientations in finite element models of the ply, which are virtually tested in longitudinal tension. Monte Carlo simulations were performed to evaluate the effect of different sources of material variability, i.e. local fibre strength, fibre volume fraction and misalignment. Ply strength predictions lowered when including the variability of local volume fraction and fibre misalignment in the modelling, showing a better agreement with experiments for the carbon/epoxy system investigated.

Keywords:
Lamina/ply, Strength, Statistical properties/methods, Finite element analysis (FEA)

1. Introduction

Unidirectional carbon fibre composites show their best performance when loaded in longitudinal tension. Nevertheless, due to the intrinsic complexity of the material, the material properties present a large variability [1–4].

In the aerospace field, where safety and lightweight are crucial, material basis values (or material allowables) are used to ensure material reliability [5]. The identification of material basis values require extensive experimental campaigns, with a minimum of 30 tests per condition for B-basis values (which correspond to 90% reliability) and of 90 tests per condition for A-basis values (ensuring 99% reliability) [5]. In other industrial applications, large number of tests are often not possible due to the high cost. The resulting uncertainty of the material strength leads to overdesigned components.

Strength of unidirectional materials can be characterized by a typical scatter of about 3%, which can be as high as 12% [6]. Such scatter may be due to variations in the properties of the constituents (e.g fibre strength), as well as in the material quality deriving from manufacturing (e.g. fibre misalignment or local variability of volume fraction).

In this context, virtual material characterisation becomes attractive as a tool to predict material properties and their variability [7–9]. This can lead to reduced safety factors and consequently improve manufacturing time and cost.

*Corresponding author
Email address: fabio.malgioglio@siemens.com (Fabio Malgioglio)

Several fibre break models were developed in the literature (e.g. in [10–13]) to predict longitudinal tensile failure of impregnated fibre bundles. Most fibre break models combine Weibull statistics [14] for fibre failure (popular for brittle reinforcements, like carbon and glass fibres) with stress intensifications occurring in intact fibres surrounding a fibre break.

In this way, the models try to replicate the development and growth of clusters of broken fibres, observed experimentally by means of X-ray micro computed tomography (μCT) [10, 15–17]. However, most models struggle to predict the accumulation of fibre breaks in composite bundles correctly [18].

One common modelling assumption that might decrease the accuracy of fibre break models is the assumption that V_f is uniform in the material, coinciding with a nominal value. In some models [10, 13], the randomicity of fibre arrangement is included, based on random packing generators (e.g. [19]). Even random packings, however, are generated targeting a nominal V_f, with limited variability at very short range (few fibres distance). However, due to the manufacturing, V_f is not uniform in the material [20], i.e. V_f is not the same in different locations.

A non-uniform V_f also implies a different distribution of material properties, which is often neglected in modelling longitudinal tension. In contrast, the effect of local fibre volume fraction variability was shown to influence the failure behaviour in the transverse direction in unidirectional composites [4, 21].

Fibre misalignment, which is an important factor affecting compressive strength [22–24], is rarely modelled for longitudinal tension. In fact, most fibre break models consider the fibres straight and parallel, which is not the case in real materials [25–27].

Fibre misalignment can be modelled explicitly at the microscale when μCT data at high resolution are available [26] or with a randomly generated geometry [28] (as it was recently done in [29]). This, however, may require significant computational resources and limit the modelling to relatively small volumes. Moreover, spatial variability of fibre misalignment, present in the material at the scale of few millimetres [27], would not be considered.

Due to the assumptions and limitations of fibre break models, it is challenging to model the effect of local fibre volume fraction and fibre misalignment variability. A possible solution (suggested in [18]) could be to use a fibre break model in a multiscale framework.

A first step towards including material variability in longitudinal tensile strength predictions of unidirectional (UD) plies was done in a previous research [30]. There, local material strength was derived using the fibre break model by Swolfs et al. [10]. This approach, however, suffered from the computational time required for the fibre break model to run, limiting the model versatility.

This paper proposes a model for the identification of longitudinal tensile failure in UD plies and its variability under longitudinal tension. The model is used to evaluate the effect of material variability on the longitudinal tensile strength predictions.

The model consists of a multiscale framework, which considers three sources of material variability, namely the fibre strength variability, local fibre volume fraction variability and local fibre misalignment.

Material variability is reproduced assigning different properties to each element, i.e. elastic properties and local material orientation. Here, local composite strength (assigned to each element according to the fibre volume fraction) is calculated with the hierarchical scaling law proposed by Pimenta and Pinho [12], exploiting its computational efficiency.

Several finite element models of a tensile specimen are generated and loaded in tension. For each simulation, longitudinal tensile strength, strain to failure and longitudinal tensile modulus are extracted.

To evaluate the effect of fibre strength statistics combined with fibre misalignment and local fibre volume fraction variability, a large virtual testing campaign is performed (using the Monte Carlo method) on two different materials, which differ in variability (resulting from different manufacturing processes). Finally, simulation results are compared with experiments from the literature [31].

The calculation of local fields of material properties, i.e. V_f, misalignment and strength, and how they are assigned to the virtual material is explained in section 2. Section 3 deals with the virtual testing methodology. Here, the modelling strategy used in the paper are described in detail. Results are presented in section 4. In section 5, the main advantages and limitations of the model are discussed. Finally, conclusions of the paper are drawn in section 6.

2. Virtual representation of a composite UD ply

A way to capture the material variability in the ply is to subdivide it in smaller volumes. In each volume, V_f and preferential fibre orientation can be measured, for example with μCT, and statistical characteristics of the variability derived. To reproduce the variability, the UD ply was modelled with a thin, rectangular cuboid shaped finite element model.

The size of the finite elements was chosen equal to the size of a portion of material, which was related to the window size used to characterise the local fibre volume fraction by mean field image analysis (as explained in more detail in section 2.3). Each finite element was modelled as an homogeneous, transversely isotropic material.

The material orientation (representing misalignment), the homogenized elastic properties (based on the properties of the constituents and V_f), and strength need to be assigned to each finite element. This section explains how these properties were calculated and assigned to the virtual material.

2.1. Studied material

The material chosen for the investigations was a carbon/epoxy system, with the properties of IM7 fibres and 8552 resin produced by Hexcel. The constituent properties considered in this paper were taken from [32, 33] and [34] for the fibres and matrix respectively. The values used are reported in Table 1.

Table 1: Properties of the constituents used in this study.

Fibre properties [32, 33]						
Elastic properties	$E_{11,f}$ $[GPa]$	275.00	$E_{22,f}$ $[GPa]$	19.00	$E_{33,f}$ $[GPa]$	19.00
	$G_{12,f}$ $[GPa]$	27.60	$G_{13,f}$ $[GPa]$	27.60	$G_{23,f}$ $[GPa]$	12.88
	$\nu_{12,f}$ $[-]$	0.20	$\nu_{13,f}$ $[-]$	0.20	$\nu_{23,f}$ $[-]$	0.35
Weibull parameters	σ_0 $[GPa]$	8.27	m $[-]$	8.81	L_0 $[mm]$	1.75
Matrix properties [34]						
Elastic properties	E_m $[GPa]$	4.67	G_m $[GPa]$	1.67	$\nu_{12,m}$ $[-]$	0.3982
Interface strength	τ_s $[MPa]$	69.3				

The effect of variability was studied on two different virtual cases, with two different levels of variability. The first case was a material with V_f and misalignment typical of a *prepreg* material (with data taken from [27] and [31]). The second case was a material with values representative of an *RTM* (resin transfer moulding) composite (taken from [27] and [20]). The prepreg material had a higher V_f and a narrower V_f distribution compared to the RTM material. This allowed to understand the effect of the modelling parameters (discussed in section 4). The modelling parameters of the two materials are listed in Table 2. It should be pointed out that the constituents from [27] and [20] are not provided and therefore may be different from the ones from [31]. Also, the correlation length parameters and volume fraction statistics were not identified from the material tested in [31]. Nevertheless, the material parameters used here (linked to the manufacturing process) allowed to study the effect of material variability, which is the scope of the paper.

2.2. Fibre misalignment

The local fibre misalignment φ is the deviation of the orientation of the fibres from the nominal orientation of the ply (expressed in degrees).

The misalignment can be measured with different techniques, such as ellipsometry [25, 35] or μCT [16, 26, 27, 36]. Although individual fibre misalignment could be modelled explicitly if μCT data at high resolution are available (e.g. data from [26]) or by generating the geometry with a random generator [28], this was not done here because it would limit the analysis to relatively small samples (i.e. to volumes of $\sim 1\,mm^3$ size).

Table 2: Table of materials parameters for V_f and misalignment for prepreg and RTM carbon/epoxy materials.

	Prepreg			RTM		
	Mean	Standard deviation	Ref.	Mean	Standard deviation	Ref.
V_f [%]	57.3	2.00* (*estimated*)	[31]	51.90	5.08	[20]
φ_{ip} [°]	0.00	1.12	[27]	0.00	1.37	[27]
φ_{op} [°]	0.00	0.70	[27]	0.00	1.63	[27]
l_{ip} [mm]	3.70	-	[27]	1.60	-	[27]
w_{ip} [mm]	0.73	-	[27]	0.73	-	[27]
l_{op} [mm]	2.40	-	[27]	1.10	-	[27]
w_{op} [mm]	0.73	-	[27]	0.73	-	[27]

Alternatively, mean field image analysis techniques allow to measure fibre misalignment (intended as the average orientation of the fibres in a predefined area) over larger areas and in more reasonable time. This would allow to evaluate the effect of spatial correlation of fibre misalignment on relatively large volumes. Among these techniques, the multiple field image analysis (MFIA) [37], Fourier transform image analysis (FTIA) [38] can be used on $2D$ images, and structure tensor analysis [39] can be used with μCT data in $3D$.

In [27], the *in-plane* and *out-of-plane* misalignment, respectively φ_{ip} and φ_{op}, were measured using MFIA from μCT images of unidirectional materials, produced with prepreg and resin transfer moulding (RTM) technology, and spatial correlation analysis was performed.

The spatial correlation length l and width w of φ_{ip} and φ_{op} were estimated using autocorrelation functions. In reference [27], the measurements were done on square windows of 300 μm side.

In this paper, the misalignment fields were generated randomly using the data from [27], following the procedure proposed in [40] (reported in Appendix A). This method allows to generate random fields with the desired properties in terms of mean, standard deviation and spatial correlation. Fields of misalignment were generated on discrete, rectangular grids, representing the finite elements of the model. The misalignment generated in each grid point was then assigned to the elements as local material orientation. By doing so, it was assumed that the homogenised material behaviour corresponded to a UD composite with fibre orientation defined by the misalignment.

Misalignment fields were generated using the correlation parameters from [27] (See Figure 1). In Figure 2, it is shown that the mean and standard deviation of misalignment used as input are correctly reproduced. The parameters required to generate the spatially correlated random field of misalignment were the misalignment mean μ_φ (equal to 0), the misalignment standard deviation Σ_φ, the correlation length l and correlation width w (for both in-plane and out-of-plane misalignment) and the grid spacing L. L was considered equal to the element size, as discussed in section 2.3.

Misalignment can be decoupled as in-plane and out-of-plane misalignment, which is also convenient for the experimental characterisation of misalignment [27]. The correlated random field generator, which is formulated in two dimensions (see Appendix A), was used sequentially to generate fields of misalignment in parallel planes (in both in-plane and out-of-plane directions). In this way, the fibre orientation in each element is composed of in-plane and out-of-plane misalignment, which are assumed independent between each other.

All the required parameters for the random generation of misalignment were measured for prepreg and RTM materials [27] and used for the present study. In [27], the spatial correlation was evaluated with the autocorrelation function. Such function shows how a set of data distributed in space (as the misalignment in this study) is similar to itself, when shifted in space. When the shift is null, i.e. when the data set is identical to the shifted one, the correlation is perfect and the autocorrelation function is equal to 1. For a long space shift, the autocorrelation function tends to zero. If the autocorrelation function tends to zero quickly, then the data are not spatially correlated. Otherwise, data are correlated in space and a correlation length can be defined.

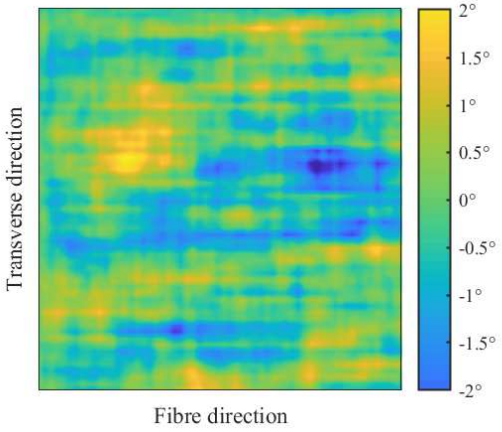

Figure 1: Random realization of in-plane misalignment field, generated with the algorithm from [40]. The area considered here is of $4.2\,mm \times 4.2\,mm$.

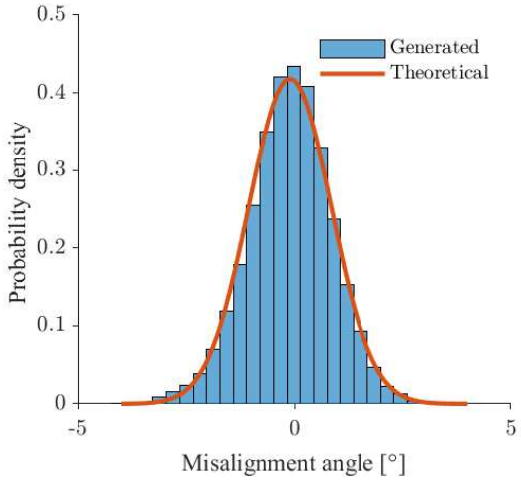

Figure 2: Verification of statistics of a random realization of misalignment vs. the theoretical normal distribution.

In [27], the correlation length was defined as the length for which the autocorrelation function became smaller than a threshold value, equal to 0.1. The so defined correlation length $l_{0.1}$ needed to be modified into l_{mod} to be used in the random field generator according to (1), to be consistent with its exponential formulation:

$$l_{mod} = -\frac{l_{0.1}}{ln(0.1)} \tag{1}$$

with ln being the natural logarithm.

2.3. Spatial correlation of V_f

The variability of V_f in the transverse direction can be assessed with image analysis techniques. Sanei and Fertig III studied the spatial correlation of V_f on images of transverse sections of unidirectional composites [20]. The cross-correlation between V_f in a window of a given size and the surrounding space was calculated. The window size was increased until the cross-correlation between neighbour windows was small enough to be considered uncorrelated. Once the uncorrelated window size had been defined, the distribution of V_f was calculated and sampled to randomly assign V_f to elements in stochastic modelling. This concept of "uncorrelated volume element" used in [20] was also used here. In [20], a window size of $70\,\mu m$ side for uncorrelated V_f was identified. In general, the uncorrelated window size depends on the particular material considered, including the fibre diameter, the nominal fibre content and the manufacturing process. In this paper, the window size was not measured and was kept equal to $70\,\mu m$ in first approximation.

For the chosen window size, it was possible to randomly sample V_f from the probability distribution corresponding to that window size (given in [20]). In contrast to the transverse direction, the correlation of V_f was assumed to be very strong in the longitudinal direction, due to the continuity of fibres. V_f is assigned to the virtual ply in two steps. First, V_f is assigned randomly (based on a probability distribution with the parameters given in Table 2) to the first transverse section of the ply and propagated with no modification to all the other sections. Then, V_f is corrected by adding a spatially-correlated random field of volume fraction variation ΔV_f, which is calculated with the same procedure used for misalignment, as reported in detail in Appendix A. An example of the mapping of V_f on the virtual ply is presented in Figure 3.

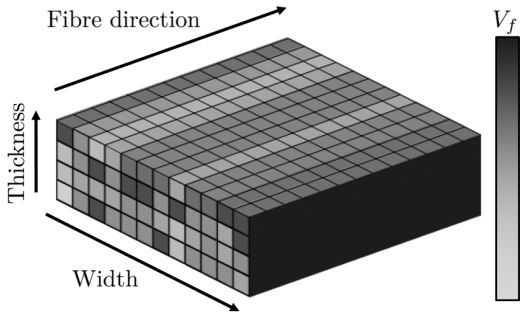

Figure 3: Example of V_f mapping on a virtual coupon.

In first approximation, it was assumed that the correlation length for ΔV_f in the longitudinal direction was equal to the one of in-plane misalignment l_{ip}. The correlation width w was set to close to zero, so that the generated field was not correlated in the transverse direction (see Appendix A for further details).

2.4. Local material properties

Misalignment and V_f values were generated and assigned to all material locations, as described in sections 2.2 and 2.3. This information was then translated in material properties and assigned to the finite element model. In this paper, the mechanical behaviour of each element was assumed perfectly linear elastic up to failure. This assumption can be justified by the fact that very small non-linearities are reproduced by fibre break models [18]. Typically, carbon fibres exhibit a non-Hookean behaviour (i.e. stiffening of carbon fibres with the applied strain [41]), which is neglected here.

Also, it was assumed that, locally (i.e. in the volume of a finite element), the homogenised material had the same behaviour of a UD composite with fibres orientation defined by the misalignment. Under these conditions, the elastic properties were calculated according to Chamis' homogenization rules [42] based on the local V_f and the elastic properties of the constituents. The local $3D$ misalignment was assigned to each element rotating the material orientation system, based on the information of the local in-plane and out-of-plane misalignment (φ_{ip} and φ_{op} respectively).

Local values of composite longitudinal tensile strength were calculated using a fibre break model. The hierarchical scaling law proposed by Pimenta and Pinho [12, 43] was used to predict the probability distribution of longitudinal tensile strength a bundle of impregnated, parallel fibres. This model provided good results in comparison with experiments at very low computational cost [18]. The main phenomena occurring during failure, such as the stress recovery along the broken fibres, yielding of the matrix or fibre-matrix interface and stress concentrations around the fibre breaks are considered. In the hierarchical scaling law, the failure probability of single fibres (described with Weibull statistics) is propagated iteratively to fibre bundles of 2, 4, 8, $\cdots$, 2^n fibres, to give the strength probability distribution of the fibre bundle (normalized by the cross sectional area of the fibres). The composite strength can be obtained with the rule of mixtures, which incorporates both the contribution of fibres and matrix. V_f is taken into account in the hierarchical scaling law as a geometrical parameter that defines the inter-fibre distance.

In this paper, the hierarchical scaling law is used to calculate the strength probability distributions of fibre bundles of the dimension of a finite element (discussed in section 2.3), with different V_f. For a bundle of given volume, V_f is linked to the number of fibres n_f, which is, in general, different from a power of 2. Therefore, the probability distributions were first calculated for bundles of 2^i fibres, with $i = 1, 2, ..., n$ and given V_f. Then, the distributions were interpolated to the correct value of n_f, corresponding to V_f, using a spline interpolation. This process is repeated for a range of different V_f.

Assuming that the fibres have a uniform and fixed cross-sectional area A_f, then the number of fibres in a bundle n_f, the fibre volume fraction V_f, and the cross-sectional area of a bundle A_b are

related by the following equation:

$$A_b = n_f \cdot A_f \cdot V_f \tag{2}$$

Note that A_b being equal to the volume of the bundle divided by the bundle length.

Therefore, the effect of these three parameters (i.e. n_f, V_f, and A_b) will be studied separately in Figures 4-6, in order to understand their effect on the failure strain of the fibre bundle ε_f. ε_f is obtained dividing the strength value normalized on the fibre cross section by the fibre modulus.

For a fibre bundle length $L = 70\,\mu m$ and $V_f = 50\,\%$, ε_f and its standard deviation were calculated for bundles of different size n_f (Figure 4). Increasing n_f, both the mean value and standard deviation of ε_f decreased. The explanation is that increasing n_f, also the probability to find a defect able to cause failure increases. This effect is known as *size effect*.

A similar analysis was conducted keeping n_f constant and changing V_f. Here, the effect of V_f on ε_f was much less pronounced, with a slight increase of ε_f with V_f (Figure 5). It can be concluded that, with the hierarchical scaling law, V_f, i.e. the distance between the fibres in the bundle, has a much less important effect on ε_f than the size effect.

The effects of V_f and n_f were assessed together by comparing bundles with fixed volume (the volume used is a cube with $70\,\mu m$ side). Note that V_f and the number of fibres in a fixed volume are directly related, in particular higher values of V_f lead to higher n_f.

The increase of n_f in the volume led to a small decrease in ε_f (Figure 6). It must be noted that bundles of higher V_f are stiffer. Consequently, mean strength was higher in bundles of higher V_f. This can be observed in Figure 7, where the strength probability distributions of bundles of fixed volume were compared. Also, strength distributions became broader with higher V_f. This has to do with the fact that values of strength are considerably higher for higher V_f, and so is the standard deviation. When computing the coefficient of variation, it actually decreased with V_f, indicating a decrease in variability.

The hierarchical scaling law was used to calculate strength probability distributions for a broad range of V_f. The local strength was assigned to each mesh element of the UD ply by random sampling the probability distribution correspondent to the V_f of the element.

3. Virtual testing methodology

Section 2 dealt with the material variability and generation of the virtual material. In this section, the virtual testing methodology is presented. In 3.1, the size of virtual coupons, the boundary conditions and the applied load are described. In 3.2 linear analyses were used to virtually test a large number of specimens up to the first ply failure, through a Monte Carlo analysis.

3.1. Virtual testing setup

The FE model of a virtual coupon consisted of a thin, rectangular cuboid shaped geometry (see Figure 8). Solid hexahedral elements (8 nodes) were chosen. The element size measured $70\,\mu m$ in the three dimensions, based on the window size defined for the correlation of V_f (See section 2.3). The element length was kept equal to $70\,\mu m$ to ensure good aspect ratio of the solid elements. The length and width of the model were chosen equal to 120 and 60 elements respectively. Here, the size was chosen so that it contained the correlation length of misalignment several times. The thickness was chosen equal to 4 elements, as it was comparable to the thickness of a ply. The virtual coupon size was therefore $8.4\,mm \times 4.2\,mm \times 0.28\,mm$. The coupons were loaded in the fibre direction (defined as x in Figure 8) fixing one transverse face and enforcing displacement in the opposite face. The material is not uniform due to variability, causing the twisting of the ply when loaded in tension and the movement of the loaded faces in the transverse plane (y-z). This effect should be avoided, as some elements would be excessively loaded due to the twisting and bending of the specimen. Moreover, the specimen needs to be blocked in at least one node in the y and z directions to meet the isostatic condition. Where the boundary conditions on y and z are applied, stresses can be high. To partially overcome the undesired twisting and bending, the boundary conditions on y and z were chosen such

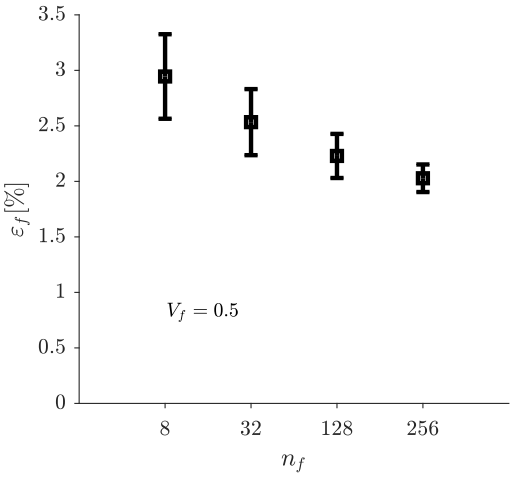

Figure 4: Effect of n_f on the strain to failure of a composite of constant V_f (and variable cross-sectional area A_b), calculated for a length of $L = 70\,\mu m$. The error bar represents the standard deviation.

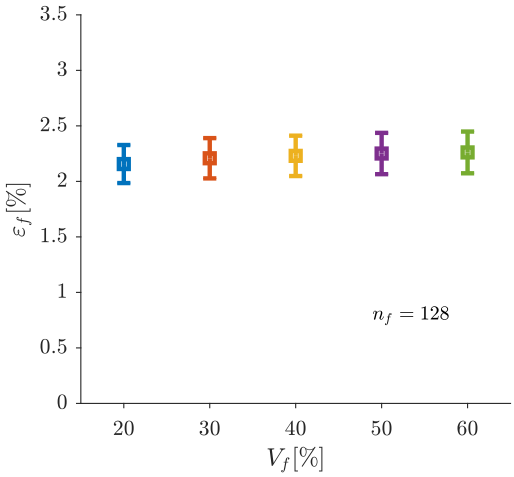

Figure 5: Effect of V_f on the strain to failure of a composite of constant n_f (and variable cross-sectional area A_b), calculated for a length of $L = 70\,\mu m$. The error bar represents the standard deviation.

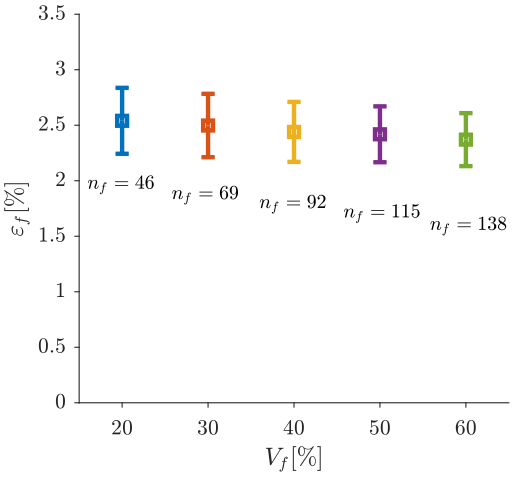

Figure 6: Effect of V_f on the strain to failure of a composite with constant cross-sectional area A_b (and variable number of fibres), calculated for a length of $L = 70\,\mu m$. The error bar represents the standard deviation.

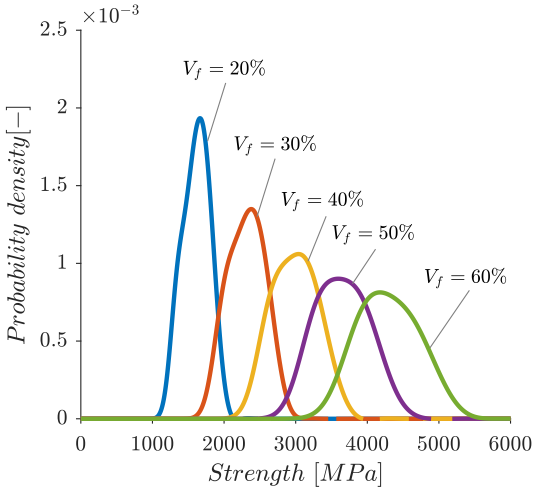

Figure 7: Failure probability of elements of different V_f, calculated for a length of $L = 70\,\mu m$.

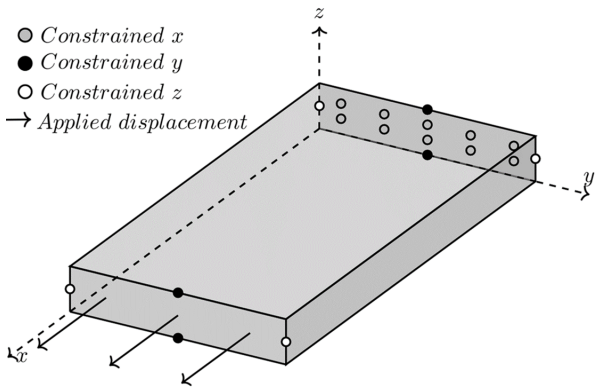

Figure 8: Qualitative representation of the virtual specimen and of the applied boundary conditions.

that the axis of the specimen remained aligned to the x direction and Poisson's contraction was allowed away from the transverse boundaries (Figure 8). For each of the two loaded faces (perpendicular to x), two pairs of nodes were selected in the centre of opposite edges. Each pair of nodes was blocked in the direction parallel to the edge they belonged (either y or z). Stress concentrations occurred close to the blocked nodes, fading rapidly away from them. To avoid failure in this perturbed zone, the strength values of the first three rows of elements close to the loaded faces were artificially increased.

3.2. Ply failure

The material behaviour of the ply was assumed linear elastic until the first element failure occurred. Linear simulations were used to reproduce the material behaviour until the first element failed. Non-linear analysis allows to account for more complex material behaviours, such as plasticity and progressive damage. Including these effects in the analysis, however, is not expected to improve strength predictions significantly, as this type of material typically behave in a brittle manner [44]. On the other hand, the advantage of linear simulations over the non-linear ones is the much lower computational cost. A large number of virtual tests were performed in a Monte Carlo fashion, allowing the study of the influence of several modelling parameters. In the linear analyses, a 1 % strain was applied to the virtual coupons. The longitudinal stresses in the elements were then extracted and compared to the corresponding strength computed beforehand with the hierarchical scaling law. The first failing element was identified as the element with the highest failure index (i.e. the stress-to-strength ratio). The failure strain of the ply was computed with a linear proportion, hence dividing the applied strain and the failure index.

4. Results and discussion

Linear analysis was used here to identify the first ply failure in the coupon and allow to study the effect of material variability, performing a high number of FE simulations in a feasible computational time. Two materials were investigated (RTM and prepreg), as described in section 3.

For the two materials, longitudinal tensile strength was predicted using both the hierarchical scaling law [12] and the FE framework described in this paper. For each case investigated with the FE model, 500 simulations were performed, which were shown to be enough to reach convergence of the mean and standard deviation of the predicted strength in a previous research [30].

For the RTM material, five different cases were investigated:

i) Hierarchical scaling law (applied to the coupon directly)

ii) Uniform coupon with no V_f variation and no fibre misalignment, but with local strength variability

iii) Coupon with V_f variation and without fibre misalignment (on top of strength variability)

Table 3: Strength results for the simulation campaign.

Material	**Source**	**Mean [MPa]**	**STD [MPa]**	**CoV**[%]
RTM	Hierarchical scaling law	2488	65	2.6
	Uniform	2503	69	2.8
	V_f variability	2494	70	2.8
	Misalignment	2467	73	3.0
	V_f variability & misalignment	2465	72	2.9
Prepreg	Experimental [31]	2559	105	4.1
	Hierarchical scaling law	2733	71	2.6
	Uniform	2743	72	2.6
	V_f variability & misalignment	2720	79	2.9

iv) Coupon without V_f variation but with fibre misalignment and strength variability

v) Coupon with V_f, fibre misalignment and strength variability

In this way, it was possible to evaluate the single contribution of each feature separately. Firstly, longitudinal tensile strength was predicted using the hierarchical scaling law applied to the whole specimen. This was done using the procedure described in section 2.4, but using the specimen size instead of the element size. The strength probability distribution obtained was sampled 500 times and the strength mean and standard deviation (presented in Table 3) calculated. The second case was the uniform coupon (i.e. with no variability of V_f and fibre misalignment) calculated with the FE model. Here, the only source of variability was the local strength, calculated for each element with the hierarchical scaling law. This case is conceptually equivalent to the one where the hierarchical scaling law was applied to the whole specimen. Strength results for these two cases (see Table 3) present a small difference, with the hierarchical scaling law delivering slightly lower results in term of mean and standard deviation. This can be attributed to the propagation of small numerical errors when applying the hierarchical scaling law to the length of one element and sampling the strength values for all the elements.

Nevertheless, the difference between these two cases is small. Modelling V_f variability in the FE model had a small effect on the predicted strength, both in terms of mean values and on standard deviation. This is in line with the small effect of V_f on the failure strain of the elements resulting from the hierarchical scaling law, as shown in Figure 6.

Modelling fibre misalignment lowered the mean value more significantly and slightly increased the strength standard deviation. Modelling material variability with the FE model (V_f variability and fibre misalignment) lowered the strength predictions of 1.5 % and increased the coefficient of variation of 6 %. Compared with the results obtained with the hierarchical scaling law, the coefficient of variation of the predicted results increased by 12 %.

For the prepreg material, three cases were studied:

i) Hierarchical scaling law (applied to the coupon directly)

ii) Uniform coupon with no V_f variation and no misalignment, but with local strength variability

iii) Coupon with V_f, misalignment and strength variability

In contrast to the RTM material, for the prepreg only the extreme cases were investigated (i.e. the uniform coupon and the case including fibre misalignment and local V_f variability). Including the intermediate cases (where V_f variability or misalignment are modelled) would lead to a similar result already obtained for the RTM material.

The simulation results obtained for the prepreg material and experimental results from [31] are presented in Table 3. The prepreg material considered in this paper is identical to the RTM one in

terms of properties of constituents, but it differs in the mean V_f, in V_f standard deviation and in the misalignment parameters (see Table 2).

Similarly to the RTM case, also here the hierarchical scaling law gave slightly lower strength predictions compared with the FE model without V_f and misalignment variability. Including V_f variability and misalignment decreased strength prediction of about 1 %, compared with the uniform coupon case, while the standard deviation increased by 11 %.

As for the RTM case, modelling material variability of the prepreg material had a small effect on the predicted strength. One reason for this is that fibre misalignment variability is rather small for the material considered (indicating high quality of the manufacturing process). Another reason is the small effect of local V_f on the local strain to failure, as shown in Figure 6, which is a consequence of the fibre break model used.

Compared to the experimental results, all the three cases overpredicted strength of 6.8 %, 7.2 %, 6.3 % respectively.

Experimental artefacts (for example due to the effect of clamping of the specimen to the tensile machine, or due to errors in the alignment of the specimen) is not modelled in this paper. This could partially explain the strength overprediction. Nevertheless, the best results were obtained with the FE model that included material variability, both in terms of mean strength and strength variability.

5. Advantages and limitations of the FE model

This paper proposed a multi-scale strategy to predict longitudinal tensile properties of UD plies with FE models. The method exploits the predictive capabilities and computational efficiency of the hierarchical scaling law at the microscale, although incorporating its limitations and assumptions, discussed in [18]. The FE model enriches the analysis with material variability, which would be otherwise not considered by the fibre break model. The model captures variability of V_f and misalignment, although misalignment of the individual fibres is not modelled explicitly in this paper. The model generates virtual specimens that are statistically equivalent to real materials, both in terms of distributions and spatial correlation. All the parameters required by the model represent a physical quantity that can be measured from real materials (or estimated) and that can be linked to a particular manufacturing process. The virtual specimen size can be significantly larger (e.g. in the scale of cm or more) than the volume considered by some fibre break models (e.g. [10], [11] and [13]), while capturing the variability of the material, always present at a lower scale. The element shape used in this paper is rectangular cuboid. This makes the identification of the number of fibres in the elements and the fibre length straightforward (note that these two parameters are crucial in the determination of local strength). The use of more complex element shapes is also possible, if an equivalent number of fibres and fibre length are calculated in each element. Although cubic elements of 70 μm side were chosen here (see section 2.3), the model is flexible in the choice of the element size. In this paper, longitudinal fibre tension is the only failure mode considered. This assumption is valid for the low level of misalignment of the studied materials. If other failure modes are likely to occur (e.g. for a higher level of misalignment or different ply orientation) the FE model could still be used, if other failure criteria are included. Moreover, if suitable microscale models are used, the framework proposed here could be extended to different loading scenarios, e.g. longitudinal compression. Finally, the model doesn't take into account the experimental artefacts, like errors in the alignment of the specimen on the test machine.

6. Conclusions

This paper proposed a finite element framework to predict longitudinal tensile strength of unidirectional CFRPs, based on sequential multi-scale modelling. Finite element models representing composite plies were generated and used for virtual testing in longitudinal tension. The hierarchical scaling law [12] was adopted to compute the local material strength of each finite element, including

the physics of fibres breaking at the microscale. Variability of V_f and misalignment was included in the model, by means of spatially-correlated random fields, based on statistics of real materials measured in the literature. To study the effect of material variability, several hundreds of simulations were performed on two different materials, representing an RTM and prepreg ply respectively. The simulation results were compared with the predictions obtained with the hierarchical scaling law and with experimental results available in the literature. The following outcomes result from this paper:

- Including more variability factors in the analysis (i.e. variability of V_f and fibre misalignment) decreases the predicted longitudinal strength of the composite plies, with fibre misalignment being the predominant one. The strength prediction obtained with the FE model decreased by 1.5 % for the RTM material and by 1.0 % for the prepreg, compared with the case of uniform V_f and no fibre misalignment.
- Including material variability increases the scatter of the results, compared with the case of uniform V_f and no misalignment. The standard deviation increased by 4 % in the case of the RTM and by 10 % in the case of prepreg. Modelling material variability resulted in an increase in strength coefficient of variation of 12 % compared with the hierarchical scaling law.
- The comparison between experimental results from the literature [31] and the simulations showed an overprediction of 6.3 % for the tensile strength. Including the material variability in the modelling reduced the gap between simulations and experiments.

Acknowledgements

The research leading to these results has been done within the framework of the FiBreMoD project and has received funding from the European Union's Horizon 2020 research and innovation programme under the Marie Skłodowska-Curie grant agreement No 722626. S. Pimenta also acknowledges the support from the Royal Academy of Engineering in the scope of her Research Fellowship on 'Multiscale discontinuous composites for large scale and sustainable structural applications' (2015–2019). S. V. Lomov holds Toray Chair for Composite Materials at KU Leuven, support of which is acknowledged.

Appendix A. Generation of spatially-correlated random fields

In this section, the generator for random fields of misalignment and V_f is described. The theoretical background can be found in [40]. The algorithm generates a spatially correlated two-dimensional Gaussian random field on a two-dimensional grid (see Figure A.9). The generated field has zero mean and a predefined standard deviation Σ. The random fields are generated to a given rectangular grid $N_x \times N_y$, where N_x and N_y are the number of grid points in the x and y directions respectively, where x is the fibre direction and y the transverse direction.

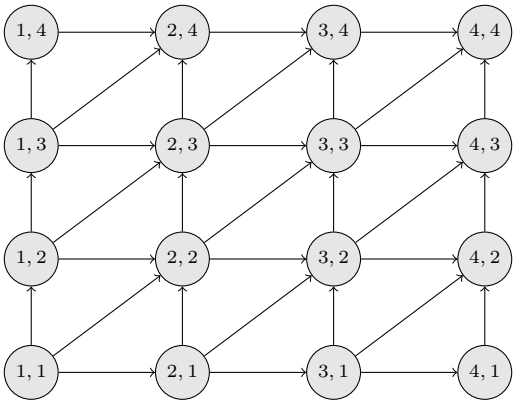

Figure A.9: Scheme of random generator used for misalignment fields in an $x-y$ plane.

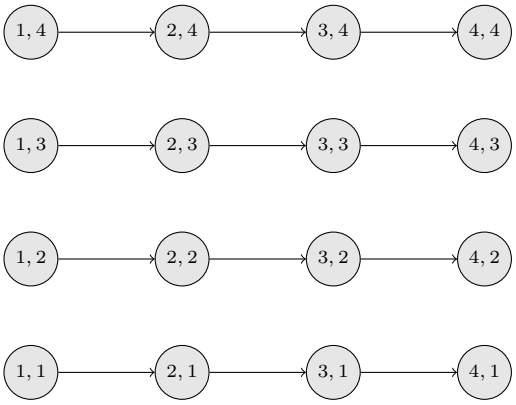

Figure A.10: Scheme of random generator used for ΔV_f fields in an $x-y$ plane.

The correlation function is given by:

$$\rho(\Delta x, \Delta y) = e^{-\Delta x/L_x} \cdot e^{-\Delta y/L_y} = e^{-\delta x \cdot n_x/L_x} \cdot e^{-\delta y \cdot n_y/L_y} \tag{A.1}$$

where Δx and Δy are the distances, δx and δy are the grid spaces, L_x and L_y are the correlation distance constants, which in this work are taken equal to the correlation lengths and widths respectively. The exponential terms for correlation r and s are introduced in equation A.2:

$$r = e^{-\delta x/L_x}, \ s = e^{-\delta y/L_y} \tag{A.2}$$

r and s only depend on the size of the grid and on the correlation length parameters. For the case of misalignment, a random value φ is given to the first grid point:

$$\varphi(1,1) = \mathcal{N}(0, \Sigma_\varphi) \tag{A.3}$$

where $\mathcal{N}(\mu, \Sigma)$ is a random number sampled from a normal distribution with mean μ and standard deviation Σ. The values are assigned to the other grid points sequentially as follows:

$$\varphi(2,1) = r \cdot \varphi(1,1) + \mathcal{N}(0, \Sigma'_\varphi) \tag{A.4}$$

$$\varphi(1,2) = s \cdot \varphi(1,1) + \mathcal{N}(0, \Sigma'_\varphi) \tag{A.5}$$

$$\varphi(2,2) = r \cdot \varphi(1,2) + s \cdot \varphi(2,1) - rs \cdot \varphi(1,1) + \mathcal{N}(0, \Sigma'_\varphi) \tag{A.6}$$

where Σ'_φ is a modified standard deviation given by A.7:

$$\Sigma^2_\varphi = (1-r^2)(1-s^2)\Sigma'^2_\varphi \tag{A.7}$$

For a general grid point (i, j), the value is given by A.8:

$$\varphi(i,j) = r \cdot \varphi(i-1,j) + s \cdot \varphi(i,j-1) - rs \cdot \varphi(i-1,j-1) + \mathcal{N}(0, \Sigma'_\varphi) \tag{A.8}$$

A similar procedure is used to construct random fields of V_f. V_f is assigned randomly to every element in the first transverse section. V_f in the first element is generated as follows:

$$V_f(1,1) = \mathcal{R}(\mu_{V_f}, \Sigma_{V_f}) \tag{A.9}$$

where $\mathcal{R}(\mu_{V_f}, \Sigma_{V_f})$ is a random number sampled from the distribution of V_f in the transverse plane (discussed in section 2.3) with mean μ and standard deviation Σ. This values of V_f are applied to all

the other sections in the longitudinal direction. To include V_f variability in the longitudinal direction, a field of V_f variation ΔV_f is generated similarly to the misalignment.

$$\Delta V_f(1,1) = \mathcal{N}(0, \Sigma_{\Delta V_f}) \tag{A.10}$$

In this paper, V_f was considered correlated in the longitudinal direction only (see section 2.3). To include this, the correlation length in the transverse direction L_y is considered small, so the contribution in the transverse direction (given by the term s from equation A.2) becomes negligible. This is shown schematically in Figure A.10. ΔV_f is propagated in the longitudinal direction as:

$$\Delta V_f(i,j) = r \cdot \Delta V_f(i-1,j) + \mathcal{N}(0, \Sigma'_{\Delta V_f}) \tag{A.11}$$

with Σ' defined as in A.7. The field of V_f through the longitudinal direction is obtained summing the V_f field of equation A.9 with the field of ΔV_f of equation A.11.

References

[1] T. Philippidis, D. Lekou, D. Aggelis, Mechanical property distribution of cfrp filament wound composites, Composite Structures 45 (1) (1999) 41 – 50. doi:https://doi.org/10.1016/S0263-8223(99)00012-4.
URL http://www.sciencedirect.com/science/article/pii/S0263822399000124

[2] V. V. Silberschmidt, Effect of micro-randomness on macroscopic properties and fracture of laminates, Journal of Materials Science 41 (20) (2006) 6768–6776. doi:10.1007/s10853-006-0205-6.
URL http://link.springer.com/10.1007/s10853-006-0205-6

[3] M. Whiteside, S. Pinho, P. Robinson, Stochastic failure modelling of unidirectional composite ply failure, Reliability Engineering and System Safety 108 (2012) 1–9. doi:https://doi.org/10.1016/j.ress.2012.05.006.
URL http://www.sciencedirect.com/science/article/pii/S0951832012000890

[4] F. H. Bhuiyan, S. H. R. Sanei, R. S. Fertig, Predicting variability in transverse effective elastic moduli and failure initiation strengths in ud composite microstructures due to randomness in fiber location and morphology, Composite Structures 237 (2020) 111887. doi:https://doi.org/10.1016/j.compstruct.2020.111887.
URL http://www.sciencedirect.com/science/article/pii/S0263822319314825

[5] M. Handbook-MIL-HDBK, 17-1F: Composite Materials Handbook, Volume 1-Polymer Matrix Composites Guidelines for Characterization of Structural Materials, US Department of Defense.

[6] R. Degenhardt, A. Kling, A. Bethge, J. Orf, L. Kärger, R. Zimmermann, K. Rohwer, A. Calvi, Investigations on imperfection sensitivity and deduction of improved knock-down factors for unstiffened CFRP cylindrical shells, Composite Structures 92 (8) (2010) 1939–1946. doi:http://doi.org/10.1016/j.compstruct.2009.12.014.

[7] L. Farkas, K. Vanclooster, H. Erdelyi, R. Sevenois, S. V. Lomov, T. Naito, Y. Urushiyama, W. V. Paepegem, Virtual material characterization process for composite materials: an industrial solution, in: 17th European Conference on Composite Materials (ECCM17), 2016.

[8] K.-Q. Li, D.-Q. Li, P.-T. Li, Y. Liu, Meso-mechanical investigations on the overall elastic properties of multi-phase construction materials using finite element method, Construction and Building Materials 228 (2019) 116727. doi:https://doi.org/10.1016/j.conbuildmat.2019.116727.
URL http://www.sciencedirect.com/science/article/pii/S0950061819321452

[9] K.-Q. Li, D.-Q. Li, Y. Liu, Meso-scale investigations on the effective thermal conductivity of multi-phase materials using the finite element method, International Journal of Heat and Mass Transfer 151 (2020) 119383.

[10] Y. Swolfs, H. Morton, A. E. Scott, L. Gorbatikh, P. A. S. Reed, I. Sinclair, S. M. Spearing, I. Verpoest, Synchrotron radiation computed tomography for experimental validation of a tensile strength model for unidirectional fibre-reinforced composites, Composites Part A: Applied Science and Manufacturing 77 (2015) 106–113. doi:http://dx.doi.org/10.1016/j.compositesa.2015.06.018.

[11] A. Thionnet, H. Y. Chou, A. Bunsell, Fibre break processes in unidirectional composites, Composites Part A: Applied Science and Manufacturing 65 (2014) 148–160. doi:10.1016/j.compositesa.2014.06.009.

[12] S. Pimenta, S. T. Pinho, Hierarchical scaling law for the strength of composite fibre bundles (jun 2013). doi:https://doi.org/10.1016/j.jmps.2013.02.004.

[13] R. P. Tavares, F. Otero, J. Baiges, A. Turon, P. P. Camanho, A dynamic spring element model for the prediction of longitudinal failure of polymer composites, Computational Materials Science 160 (January) (2019) 42–52. doi:10.1016/j.commatsci.2018.12.048.

[14] W. Weibull, A statistical distribution function of wide applicability, Journal of applied mechanics 103 (1951) 293–297.

[15] A. E. Scott, M. Mavrogordato, P. Wright, I. Sinclair, S. M. Spearing, In situ fibre fracture measurement in carbon-epoxy laminates using high resolution computed tomography, Composites Science and Technology 71 (12) (2011) 1471–1477. doi:10.1016/j.compscitech.2011.06.004.

[16] C. Breite, E. Schöberl, M. N. Mavrogordato, L. Gorbatikh, S. V. Lomov, Y. Swolfs, Automated image analysis of ultrafast synchrotron CT scans to experimentally characterize the fibre break development during in-situ tensile tests, in: ICCM22 22nd International Conferences on Composite Materials, Melbourne, 2019.
URL `https://lirias.kuleuven.be/retrieve/545076`

[17] S. Rosini, M. N. Mavrogordato, O. Egorova, E. S. Matthews, S. E. Jackson, S. Mark Spearing, I. Sinclair, In situ statistical measurement of local morphology in carbon-epoxy composites using synchrotron X-ray computed tomography, Composites Part A: Applied Science and Manufacturing 125 (July) (2019) 105543. doi:10.1016/j.compositesa.2019.105543.

[18] A. Bunsell, L. Gorbatikh, H. Morton, S. Pimenta, I. Sinclair, M. Spearing, Y. Swolfs, A. Thionnet, Benchmarking of strength models for unidirectional composites under longitudinal tension, Composites Part A: Applied Science and Manufacturing 111 (June 2017) (2018) 138–150. doi:10.1016/j.compositesa.2018.03.016.

[19] A. R. Melro, P. P. Camanho, S. T. Pinho, Generation of random distribution of fibres in long-fibre reinforced composites, Composites Science and Technology 68 (9) (2008) 2092–2102. doi:10.1016/j.compscitech.2008.03.013.

[20] S. H. R. Sanei, R. S. Fertig III, Uncorrelated volume element for stochastic modeling of microstructures based on local fiber volume fraction variation, Composites Science and Technology 117 (2015) 191–198. doi:10.1016/j.compscitech.2015.06.010.

[21] S. H. R. Sanei, E. M. Jensen, R. S. Fertig, Multiscale stochastic analysis of FRP based on variability in fiber volume fraction, epoxy stiffness and strength, in: 56th AIAA/ASCE/AHS/ASC Structures, Structural Dynamics, and Materials Conference, no. January, 2015. doi:10.2514/6.2015-1361.

[22] D. Wilhelmsson, R. Talreja, R. Gutkin, L. Asp, Compressive strength assessment of fibre composites based on a defect severity model, Composites Science and Technology 181 (February) (2019) 107685. doi:10.1016/j.compscitech.2019.107685.

[23] N. Safdar, B. Daum, R. Rolfes, Stochastic Compressive Failure Surface Modelling for the Unidirectional Fibre Reinforced Composites under Plain stress (June).
URL http://www.eccm-ecfd2018.org/admin/files/fileabstract/a666.pdf

[24] S. L. Lemanski, J. Wang, M. P. Sutcliffe, K. D. Potter, M. R. Wisnom, Modelling failure of composite specimens with defects under compression loading, Composites Part A: Applied Science and Manufacturing 48 (1) (2013) 26–36. doi:10.1016/j.compositesa.2012.12.007.

[25] S. W. Yurgartis, Measurement of small angle fiber misalignments in continuous fiber composites, Composites Science and Technology 30 (4) (1987) 279–293. doi:https://doi.org/10.1016/0266-3538(87)90016-9.

[26] M. J. Emerson, K. M. Jespersen, A. B. Dahl, K. Conradsen, L. P. Mikkelsen, Individual fibre segmentation from 3D X-ray computed tomography for characterising the fibre orientation in unidirectional composite materials, Composites Part A: Applied Science and Manufacturing 97 (2017) 83–92. doi:http://dx.doi.org/10.1016/j.compositesa.2016.12.028.

[27] M. P. F. Sutcliffe, S. L. Lemanski, A. E. Scott, Measurement of fibre waviness in industrial composite components, Composites Science and Technology 72 (16) (2012) 2016–2023. doi:https://doi.org/10.1016/j.compscitech.2012.09.001.

[28] G. Catalanotti, T. A. Sebaey, An algorithm for the generation of three-dimensional statistically Representative Volume Elements of unidirectional fibre-reinforced plastics : Focusing on the fibres waviness, Composite Structures 227 (June) (2019) 111272. doi:10.1016/j.compstruct.2019.111272.

[29] L. Varandas, G. Catalanotti, A. Melro, R. Tavares, B. Falzon, Micromechanical modelling of the longitudinal compressive and tensile failure of unidirectional composites: The effect of fibre misalignment introduced via a stochastic process, International Journal of Solids and Structures 203 (2020) 157 – 176. doi:https://doi.org/10.1016/j.ijsolstr.2020.07.022.
URL http://www.sciencedirect.com/science/article/pii/S0020768320302997

[30] F. Malgioglio, F. Mesquita, C. Breite, A. Matveeva, L. Farkas, W. Desmet, S. V. Lomov, Y. Swolfs, Prediction of Tensile Stiffness and Failure of Carbon Fibre Composite Laminae : a Multi-Scale Non-Deterministic Approach, in: Proceedings of ECCM18 - 18th European Conference on Composite Materials, Athens, 2018.
URL https://lirias2repo.kuleuven.be/rest/bitstreams/521411/retrieve

[31] K. Marlett, Y. Ng, J. Tomblin, Hexcel 8552 IM7 unidirectional prepreg 190 gsm & 35% RC qualification material property data report, National Center for Advanced Materials Performance, Wichita, Kansas. Test Report CAM-RP-2009-015, Rev. A (2011) 1–238.

[32] H. Qian, A. Bismarck, E. S. Greenhalgh, M. S. P. Shaffer, Carbon nanotube grafted carbon fibres: A study of wetting and fibre fragmentation, Composites Part A: Applied Science and Manufacturing 41 (9) (2010) 1107–1114. doi:https://doi.org/10.1016/j.compositesa.2010.04.004.

[33] R. Gutkin, S. T. Pinho, P. Robinson, P. T. Curtis, Micro-mechanical modelling of shear-driven fibre compressive failure and of fibre kinking for failure envelope generation in CFRP laminates, Composites Science and Technology 70 (8) (2010) 1214–1222. doi:10.1016/j.compscitech.2010.03.009.

[34] Hexcel, HexPly 8552 Matrix, Epoxy matrix (180 C/356 F curing) (2016) 1–6.

[35] A. L. Stewart, A. Poursartip, Characterization of fibre alignment in as-received aerospace grade unidirectional prepreg, Composites Part A: Applied Science and Manufacturing 112 (April) (2018) 239–249. doi:10.1016/j.compositesa.2018.04.018.

[36] N. Q. Nguyen, M. Mehdikhani, I. Straumit, L. Gorbatikh, L. Lessard, S. V. Lomov, Micro-CT measurement of fibre misalignment: Application to carbon/epoxy laminates manufactured in autoclave and by vacuum assisted resin transfer moulding, Composites Part A: Applied Science and Manufacturing 104 (2018) 14–23. doi:10.1016/j.compositesa.2017.10.018.

[37] C. J. Creighton, M. P. Sutcliffe, T. W. Clyne, Multiple field image analysis procedure for characterization of fibre alignment in composites, Composites Part A: Applied Science and Manufacturing 32 (2) (2001) 221–229. doi:10.1016/S1359-835X(00)00115-9.

[38] K. K. Kratmann, M. P. Sutcliffe, L. Lilleheden, R. Pyrz, O. Thomsen, A novel image analysis procedure for measuring fibre misalignment in unidirectional fibre composites, Composites Science and Technology 69 (2) (2009) 228–238. doi:10.1016/j.compscitech.2008.10.020.
URL `https://linkinghub.elsevier.com/retrieve/pii/S0266353808004132`

[39] I. Straumit, S. V. Lomov, M. Wevers, Quantification of the internal structure and automatic generation of voxel models of textile composites from X-ray computed tomography data, Composites Part A: Applied Science and Manufacturing 69 (2015) 150–158. doi:10.1016/j.compositesa.2014.11.016.
URL `http://dx.doi.org/10.1016/j.compositesa.2014.11.016`

[40] J. Dolloff, P. Doucette, The sequential generation of Gaussian random fields for applications in the geospatial sciences, ISPRS International Journal of Geo-Information 3 (2) (2014) 817–852. doi:10.3390/ijgi3020817.

[41] W. H. m. Van Dreumel, J. L. m. Kamp, Non Hookean Behaviour in the Fibre Direction of Carbon-Fibre Composites and the Influence of Fibre Waviness on the Tensile Properties, Journal of Composite Materials 11 (4) (1977) 461–469. doi:10.1177/002199837701100408.

[42] C. C. Chamis, Mechanics of composite materials: past, present, and future, Journal of Composites, Technology and Research 11 (1) (1989) 3–14.

[43] S. Pimenta, A computationally-efficient hierarchical scaling law to predict damage accumulation in composite fibre-bundles, Composites Science and Technology 146 (Supplement C) (2017) 210–225. doi:https://doi.org/10.1016/j.compscitech.2017.04.018.

[44] M. Wisnom, B. Khan, S. Hallett, Size effects in unnotched tensile strength of unidirectional and quasi-isotropic carbon/epoxy composites, Composite Structures 84 (1) (2008) 21 – 28. doi:https://doi.org/10.1016/j.compstruct.2007.06.002.